2020 IEEE International Conference on Robotics and Automation (ICRA)
31 May - 31 August, 2020. Paris, France

Force-based Control of Bipedal Balancing on Dynamic Terrain with the "Tallahassee Cassie" Robotic Platform

Jason White[1], Dylan Swart[1], and Christian Hubicki[1]

***Abstract*— Out in the field, bipedal robots need to travel on terrain that is uneven, non-rigid, and sometimes moving beneath their feet. We present a force-based double support balancing controller for such dynamic terrain scenarios for bipedal robots, and test it on the robotic bipedal platform "Tallahassee Cassie." The presented controller relies on minimal information about the robot model, requiring its kinematics and overall weight, but not inertias of individual links or components. The controller is pelvis-centric, commanding pelvis positions in Cartesian space, which a model-free PD controller converts to motor torques in joint space. By commanding forces, torques, and a frontal center of pressure in this fashion, Tallahassee Cassie is capable of balancing on a variety of scenarios, from a lifting/sliding platform, to soft foam, to a sudden drop. These results show the potential for bipedal control to balance successfully despite minimal model information, the presence of large dynamic impacts–e.g., falling through trap door, and soft series-spring deflections. These results motivate future work for walking and running controllers on dynamic terrain with relatively low reliance on modeling information.**

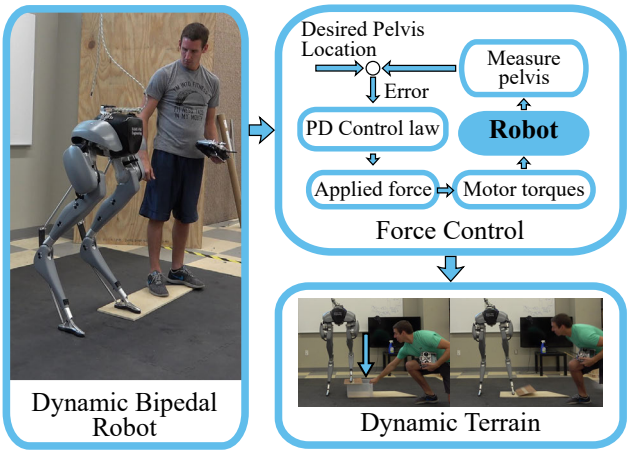

Fig. 1. We implement a force-based controller for balancing the bipedal robot, "Tallahassee Cassie" on dynamic terrain, such as soft terrain or a sudden loss of foot contact.

I. Introduction

People are capable of balancing, walking, and running out in a world where terrain is often soft and yielding–e.g., soil, sand, and snow. Sometimes, the ground moves by giving way beneath our feet, where contact points slip away under a load. Stepped-on foliage can break and rocks can roll away, robbing a biped of its precious contact forces. In these cases, the previously grounded foot must quickly find a new contact point to facilitate balance, resulting in fast ground impacts. This work presents a force-based controller to balance under these dynamic terrain effects, and demonstrates it on the bipedal robotic platform, "Tallahassee Cassie," (sometimes referred to as "Cassie") as depicted in Fig. 1. Additionally, we show the degree to which stable control is feasible using limited information about the dynamic model of the robot.

The conceptual pillar of bipedal balancing is the Zero-Moment Point (ZMP) [1] and its popular embodiment in Preview Control [2]. By guaranteeing that the ZMP resides within a robot's support polygon, the robot will not tip over. These core foundations have been greatly extended in the ensuing decades to handle a variety of uneven surfaces and partial footholds [3]. A next-generation approach to humanoid locomotion planned and controlled its joint motions using the concept of centroidal momentum. Some DARPA Robotics Challenge (DRC) humanoids using centroidal momentum could perform vehicle egress maneuvers while the vehicle was being actively bounced [4] - a form of dynamic terrain. Some DRC methods adjusted for unintended robot compliance by modeling it as a quasistatic error [5].

To extend the capability of humanoids, control methods for these fully-actuated machines have been adapted in various ways to explicitly accommodate for deformable contact. Some of these methods work by modeling the deformation and informing the control accordingly. One mode of contact deformation was demonstrated with soft shoe soles, where a deformation model enabled trajectory generation for walking [6]. The humanoid, DURUS, which bore a soft spring in its foot, was controlled via a full-order model-based optimization of the built-in compliant dynamics [7]. A physics-based modeling approach enabled planar bipedal walking on granular media (using poppy seeds as an experimental sand proxy) by modeling and exploiting measured properties of granular materials [8], and some work even uses machine learning to estimate the properties of ground-contact in-situ [9],[10],[11].

Other fully-actuated methods handle deformable contact through various forms of force/torque control for which the terrain properties need not be modeled. A ZMP approach on soft terrain, implemented on WABIAN-2R [12], uses an estimate of the robot's foot roll and torque control to correct its balance as the ground deforms. Taking a more-general force/torque control approach, NASA's Valkyrie is built with series compliance to enable torque control [13], and DLR's TORO robot [14] was torque-controlled to balance on soft gymnasium mats [15], showing robustness to soft terrain.

[1]Jason White, Dylan Swart, and Christian Hubicki are with the Mechanical Engineering Department, FAMU-FSU College of Engineering, 2003 Levy Ave., Tallahassee, FL USA jw18dn@my.fsu.edu, ds17h@my.fsu.edu, hubicki@eng.famu.fsu.edu

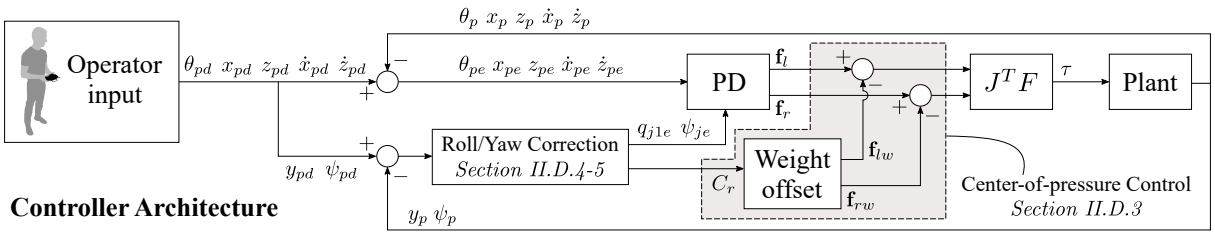

Fig. 2. Overview of control structure detailed in Section II.

Each of these approaches use highly geared motors and torque sensors to enable force control, limiting their ability to handle dynamic impacts.

Some researchers are achieving force-controlled locomotion with more dynamic impacts by using hardware without the full actuation typical of humanoids. The ongoing work through the HUME and Mercury series point-foot bipeds has shown balancing on uneven surfaces in the sagittal plane [16] and the use of stepping to balance in 3D [17]. They do so using a whole-body variant of operational space control (OSC) [18] which uses a full-body dynamic model of the robot to control task-space forces. Other legged platforms such as quadrupeds have implemented force control methods that functioned through the dynamic impacts of trotting [19] and slippery surfaces [20].

Finally, multiple control methods methods have been applied to control the Cassie series of robots from Agility Robotics (to which Tallahassee Cassie belongs). Firstly, Cassie's predecessor robot, ATRIAS/MARLO, was controlled to walk in a variety of soft outdoor terrains using control based on reduced-order models [21] and a combined hybrid-nonlinear/machine-learned policy [22]. Methods for controlling Cassie robots to walk include deep reinforcement policy learning [23] and feedback control based on reduced-order models [24]. Using control outputs that are kinematically defined, "Cassie Blue" was able to stand on uneven surfaces and walk on a variety of outdoor terrains [25]. The Cassie-series robot is notable for sporting series-springs and low-friction cycloidal drives - suitable for high-fidelity force control subject to dynamic impacts, which this work aims to exploit. *We present the ability to maintain balance in the face of soft and rapidly-moving surfaces (i.e. dynamic terrain) including foam surfaces and sudden drops while using few modeling assumptions.*

II. Methods

A. Conventions

All quantities in the body coordinate system have a left subscript **B**, and quantities without subscript are in the world coordinate system. Vectors can be identified as bold, upright, and lowercase (**p**) and matrices are bold, upright, and uppercase (**K**). Scalar values are italicized.

B. Controller Design

We treat balancing as positioning and orienting the pelvis without regard for the contact positions and achieve it with

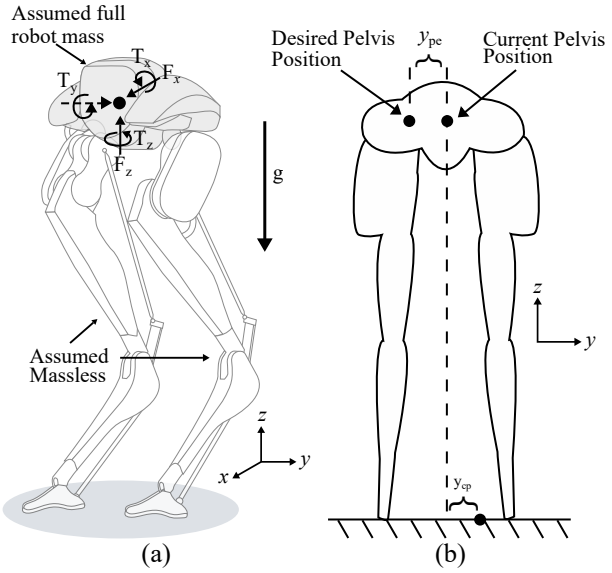

Fig. 3. (a) Cassie is controlled by commanding the listed forces and torques on the pelvis. The pelvis is assumed to be the only component with mass. (b) Cassie can regulate its y position of its pelvis by controlling the desired center of pressure.

Fig. 2. This method assumes the legs are massless, and are used only as a means to produce desired forces. This design results in a controller that is not concerned with maintaining a specific foot placement, and instead administers necessary motor torques to achieve desired pelvis orientations and positions regardless of foot placement as seen in Fig. 3. We use a traditional PD controller to command desired forces to the pelvis. The resulting desired forces are mapped in Cartesian space, and converted to motor torques through multiplication of the Jacobian transpose. We denote the current angles and positions in the world frame as

$$\mathbf{p}_i = [\phi_i \quad \theta_i \quad \psi_i \quad x_i \quad y_i \quad z_i]^T \tag{1}$$

where ϕ_i, θ_i, and ψ_i are angles about the x, y, and z axe, x_i, y_i, and z_i are the Cartesian positions, and subscripts $i \in \{p \quad r \quad l\}$ are for the pelvis, right foot, and left foot. The desired angles and positions are

$$\mathbf{p}_{id} = [\phi_{id} \quad \theta_{id} \quad \psi_{id} \quad x_{id} \quad y_{id} \quad z_{id}]^T \tag{2}$$

and are represented in the same order as current angles and positions. Subsequently, we represent the current and desired velocities using $\mathbf{v}_i$ and $\mathbf{v}_{id}$ and calculate the position and

velocity errors with $\mathbf{p}_{ie} = \mathbf{p}_i - \mathbf{p}_{id}$ and $\mathbf{v}_{ie} = \mathbf{v}_i - \mathbf{v}_{id}$. Next, we develop our gain matrices in Eq. (3), where subscript $n \in \{P \quad D\}$ denotes proportional and derivative gains.

$$\mathbf{K}_n = \begin{bmatrix} K_{n\phi} & 0 & 0 & 0 & 0 & 0 \\ 0 & K_{n\theta} & 0 & 0 & 0 & 0 \\ 0 & 0 & K_{n\psi} & 0 & 0 & 0 \\ 0 & 0 & 0 & K_{nx} & 0 & 0 \\ 0 & 0 & 0 & 0 & K_{ny} & 0 \\ 0 & 0 & 0 & 0 & 0 & K_{nz} \end{bmatrix} \tag{3}$$

The hand-tuned gains are multiplied by the errors to develop a simple PD controller. The pelvis errors are used to create desired forces for both legs to apply to the ground, so we compute two force vectors. The general equation form is

$$\mathbf{f}_j = \mathbf{K}_P \mathbf{p}_{je} + \mathbf{K}_D \mathbf{v}_{je} \tag{4}$$

where $\mathbf{f}_j$ are the torques and forces applied to the pelvis, $[T_x \quad T_y \quad T_z \quad F_x \quad 0 \quad F_z]^T$, from leg $j \in \{l \quad r\}$ as visualized in Fig. 3a. When a j subscript is present, it applies to only the left or right leg, where as the i subscript can refer to the pelvis, left leg, and right leg. Note, F_y is omitted purposefully with Cassie, where the duty of regulating y_p is allocated to a later-described center-of-pressure controller (illustrated in Fig. 3b). In Eq. (5) we develop the individual Jacobian matrix for each leg.

$${}_B\mathbf{J}_j = \begin{bmatrix} \frac{\partial({}_Bp_{j1})}{\partial(q_{j1})} & \cdots & \frac{\partial({}_Bp_{j1})}{\partial(q_{j5})} \\ \vdots & \ddots & \vdots \\ \frac{\partial({}_Bp_{j6})}{\partial(q_{j1})} & \cdots & \frac{\partial({}_Bp_{j6})}{\partial(q_{j5})} \end{bmatrix} \tag{5}$$

Here, $[q_{i1} \ldots q_{i5}]$ represents motor angles, and $[{}_Bp_{i1} \ldots {}_Bp_{i6}]^T$ represents the respective foot angles and positions in the pelvis frame (shown in Fig. 4b). The Jacobian transposes are multiplied by pelvis forces, f_j, as seen in Eq. (6) to transform individual motor torques. This is done for both the right and left legs independently.

$$\boldsymbol{\tau}_j = [\tau_1 ... \tau_5]^T = {}_B\mathbf{J}_j^T \mathbf{f}_j \tag{6}$$

Section II further details specific differences between the formulation of the force vectors and Fig. 2 is a representative visualization of the overall control scheme.

C. "Tallahassee Cassie"

Tallahassee Cassie is a Cassie series robot designed and built by Agility Robotics and inspired by natural biomechanics, as illustrated in Fig. 4. Cassie stands about 1 m tall and weighs approximately 30 kg, with each leg being about 10 kg. Each leg contains 5 motors and 2 mechanical springs. A single onboard battery provides power and allows Cassie to operate untethered and outside in unstructured environments. Cassie is operated using a radio controller, which delivers high-level user instructions. The onboard computer then uses MATLAB and Simulink to control Cassie at a rate of 2 kHz. Cassie senses the environment with a limited array of sensors. These sensors include an Inertial Measurement Unit (IMU) and joint encoders, but Cassie uses no vision nor global positioning. The in-series springs dissipate impact forces and prevent damage to the hardware, but can also be used to measure contact forces via deflection. Of the five motors on each leg, four contain cycloidal transmissions, which permit high gear reduction with low friction and no backlash. This low friction enables accurate transmission of torques, which at a high control rate enables successful force control.

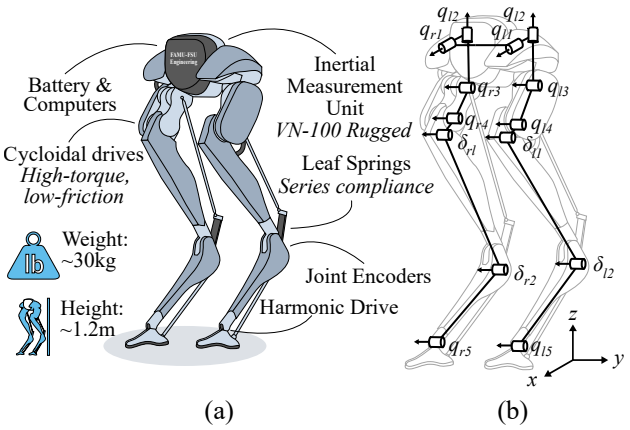

Fig. 4. (a) Overview of Cassie's hardware and basic features. (b) Kinematic diagram of Cassie showing motor positions and spring deflections.

D. Controller Implementation

We make the following key assumptions to develop the controller. First, the low friction cycloidal drives allow us to assume commanded torques are equivalent to the applied torques at the joint. For our tests, the centroid was used as the desired pelvis location as seen in Eq. (7). By centering the pelvis in the world frame, the controller is able to resist external forces up to a limit dependent upon ground slope, damping coefficient, and foot contact friction. The height of the pelvis is defined by the foot with the largest z distance as can been seen below.

$$\mathbf{p}_p = \begin{bmatrix} \phi_p \\ \theta_p \\ \psi_p \\ x_p \\ y_p \\ z_p \end{bmatrix} = \begin{bmatrix} \phi_p \\ \theta_p \\ \psi_p \\ \bar{x}_j \\ \bar{y}_j \\ max(z_j) \end{bmatrix} \tag{7}$$

To determine the angular orientation of the pelvis, or the first three values of Eq. (7), from IMU measurements. To measure the full system state, we use all fourteen encoders (seven per leg), and the IMU. After developing a symbolic expression of the forward kinematics using the MATLAB symbolic toolbox, we found the positions and angles of each foot in the world frame. We then differentiate the feet kinematics and generate a fast-solving Jacobian using the `matlabFunction` command.

1) Pelvis Velocity Measurement: The pelvis angular velocities are derived directly from IMU measurements. To determine the linear velocity, we used kinematic estimates

from both legs, combining their estimates with an average weighted by leg-spring deflections (a rough gauge of contact force magnitude). If both legs had spring deflections from contact, the pelvis' linear velocity was calculated from both feet using a weighted average based on the overall deflection,

$$\mathbf{v}_p = -\frac{\sum v_j(\delta_{j1} + \delta_{j2})}{\sum(\delta_{j1} + \delta_{j2})}. \tag{8}$$

After differentiating the forward kinematics, the computed velocity signal had problematic noise which led to motor oscillations from the derivative control terms. We apply a second-order low-pass Butterworth filter with a cutoff frequency of 10 Hz to both the linear and angular velocity derivative gain terms. To further reduce oscillation, a dead band filter to the velocity terms with a range of ± 0.10 m/s was added. After implementation, we noticed that the angular velocity gains did not contribute much to the stability, but vastly increased the probability of inducing system oscillations. This observation motivated us to set the angular velocity $\mathbf{K}_D$ gains to zero. Future work will employ an extended Kalman filter and re-implementation of these $\mathbf{K}_D$ gains.

2) Calculating Errors: The user sets the desired positions and velocities of the pelvis in the control, resulting in error between the current and desired state. The system is treated similar to a rigid body where errors at the feet are opposite of the pelvis errors. With the few exceptions discussed below, these errors are taken and multiplied by the $\mathbf{K}_P$ and $\mathbf{K}_D$ gains to compute pelvis forces.

3) Center-of-pressure Control: The Cassie series robot uses five motors to control the available six Cartesian degrees of freedom per foot. We found directly controlling all Cartesian forces except for the y force to be an effective control scheme. Instead, the y pelvis error is used to compute a desired center of pressure (y_{cp}) between the two feet as illustrated in Fig. 3b and in

$$y_{cp} = y_p - K_{cp} y_{pe} \tag{9}$$

where K_{cp} represents a new center-of-pressure gain. Using a simple statics equation we next develop a ratio that determines the necessary weight distribution per leg to achieve the desired y_{cp},

$$C_r = \frac{y_{cp} - y_r}{\sum y_j}. \tag{10}$$

When multiplied by the weight, this ratio (C_r) not only ensures the weight is always supported by the controller, but also is used to apportion vertical forces to each leg as seen in (11) and (12)

$$F_{rz} = WC_r \tag{11}$$

$$F_{lz} = W - F_{rz} \tag{12}$$

$$\mathbf{f}_{jw} = [0 \quad 0 \quad 0 \quad 0 \quad 0 \quad F_{jz}]^T \tag{13}$$

where W is an estimate of the total weight of the robot. This process is visually described in Fig. 3b.

4) Modifying x Rotation: From the center of the pelvis point to a point internal to the hip motor is a fixed distance, y_h, of 0.135 m. Then we determine whether the legs are inside or outside the form factor of the pelvis using Eq. (14). A $y_f > 0$ indicates the feet span is greater than the distance between the left and right hip points.

$$y_f = y_h - \frac{\sum \mid y_j \mid}{2} \tag{14}$$

Eq. (15) uses the y_f to determine the q_{i1} motor angles (reference Fig. 4b) necessary to induce zero roll when the pelvis is centered. These two motors are the only two directly associated with control of the pelvis roll.

$$\mathbf{q}_{j1cd} = \tan^{-1}\left(\frac{y_f}{z_j}\right) \tag{15}$$

Eq. (16) calculates the additional angles necessary for when y_d is not directly between the feet.

$$\mathbf{q}_{j1yd} = \tan^{-1}\left(\frac{y_{pd}}{z_j}\right) \tag{16}$$

Finally, we sum (15) and (16) to get the desired hip motor positions.

$$\mathbf{q}_{j1d} = \mathbf{q}_{j1yd} + \mathbf{q}_{j1cd} \tag{17}$$

The desired hip motor angles to induce zero roll were developed using the kinematic equations and IMU data. After testing, this method of control proved to be more effective than directly controlling the pelvis roll based on the IMU measurement alone.

5) Modified z rotation: In order to keep the feet from bowing in or out (yaw rotation), individual foot rotation control around the z axis is included. To simplify the controller, we set $\psi_{ld} = \psi_{rd} = \psi_{pd}$ and the feet errors are calculated in the same manner previously mentioned,

$$\boldsymbol{\psi}_{je} = \psi_{jd} - \psi_j. \tag{18}$$

6) Forces: Using the modified error calculations we compute the force vectors for the left and right foot separately. Note that the previous modifications now result in

$$\mathbf{p}_{je} = [\mathbf{q}_{j1e} \quad \theta_{pe} \quad \boldsymbol{\psi}_{je} \quad x_{pe} \quad 0 \quad z_{pe}]^T \tag{19}$$

and

$$\mathbf{v}_{je} = [0 \quad 0 \quad 0 \quad \dot{x}_{pe} \quad 0 \quad \dot{z}_{pe}]^T. \tag{20}$$

Multiplying errors by the gains and subtracting the center of pressure force yields

$$\mathbf{f}_j = \mathbf{K}_P \mathbf{p}_{je} + \mathbf{K}_D \mathbf{v}_{je} - \mathbf{f}_{jw} \tag{21}$$

The $\mathbf{K}_P$ and $\mathbf{K}_D$ gains are identical for both legs. Using Eq. 6, we find the torques necessary to drive the pelvis to the desired position. The computed torques are commanded and realized using Cassie's onboard motor controllers.

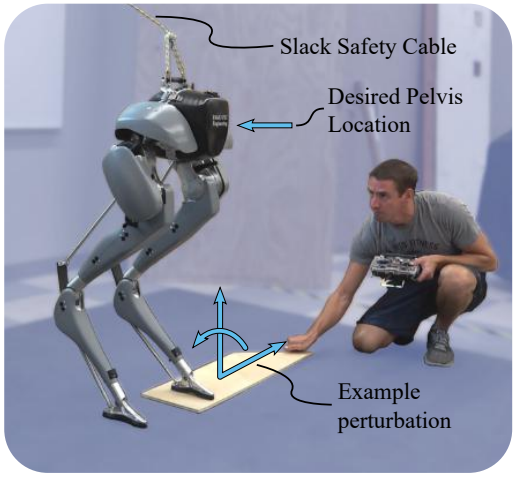

Fig. 5. Experimental setup for testing the balancing controller on Tallahassee Cassie for each of four balance perturbations.

E. Multibody Simulation

To test how the controller performs in simulation, we a multibody model of Cassie built in Simulink Multibody in MATLAB 2017b. This platform provides us with a 3D simulation that accounts for impact forces, inertia, and many other nuances present in Cassie's multibody dynamics. The overall model has the same number of joints, motors, and springs and similar masses, kinematics, and moments of inertia as estimated on Cassie. To reduce the simulation computation time the contact model utilizes spheres at the front and back of each toe for a total of four points of contact including both legs.

III. Experimental Setup

During each trial Cassie is kept on a safety harness to prevent damage in the event of failure (Fig. 5). This harness is kept slack throughout each experiment to minimize interference. Cassie is then booted and calibrated, after which power is supplied to the motors and motor torques are slowly ramped up as Cassie comes to a complete standing pose with assistance. After Cassie is standing, perturbations are applied. Then, power is cut to the motors and data stops being recorded from the onboard computer. During each trial, Cassie's onboard computer logs data at a rate of 2 kHz.

Four types of balance perturbations were applied to Cassie. The "Leg Spread" is conducted by placing a board under Cassie's foot that is used to slide Cassie's foot right and left, simulating unstable terrain. This board is also used for the "Lift and Lower" where the board is slowly lifted, causing Cassie's foot to lift and be on uneven footing, which constitutes uneven terrain. In order to simulate soft terrain in the "Soft Foam and Push," one of Cassie's feet is placed on foam mats and Cassie is given slight pushes. Then, to simulate losing a foothold in the "Box Drop," Cassie is placed with one foot on a box, and this box is quickly forced out from underneath the foot, causing that foot to fall to the ground.

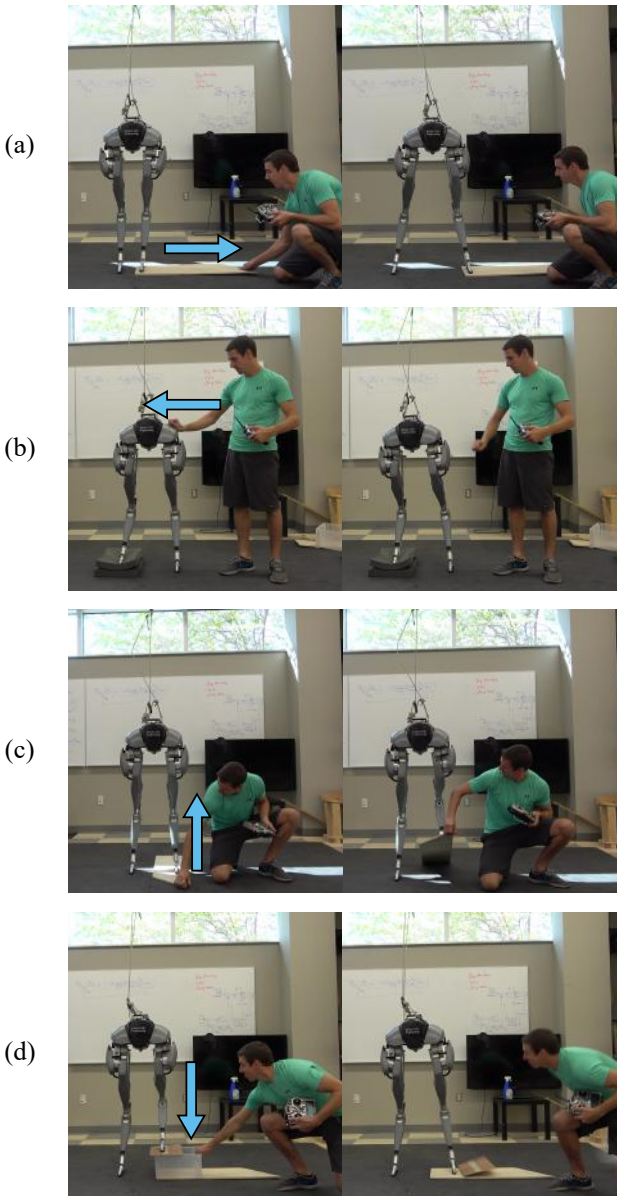

Fig. 6. Examples of different perturbations applied on Tallahassee Cassie. (a) "Leg Spread": Cassie's foot is moved by sliding a board. (b) "Soft Foam and Push": One of Cassie's feet is supported by soft foam and the pelvis is pushed. (c) "Lift and Lower": Cassie's foot is raised and lowered using a board. (d) "Box Drop": A box is quickly pulled from under Cassie's foot, forcing it to recover from a fall.

IV. Results

Each of the four perturbation scenarios are shown visually in Fig. 6 and their respective pelvis trajectories are plotted in Fig. 7. Tallahassee Cassie was able to remain balanced while (1) having its leg pulled to the side 55cm, (2) having its leg lifted vertically by 30cm, (3) standing on a soft foam and pushed, and (4) when a 17cm-tall box is pulled from under its foot. In each case, the controller accommodates the disturbance, and settles back near the desired pelvis location. These tests experimentally demonstrate the effectiveness of the simple force controller in spite of highly simplified assumptions.

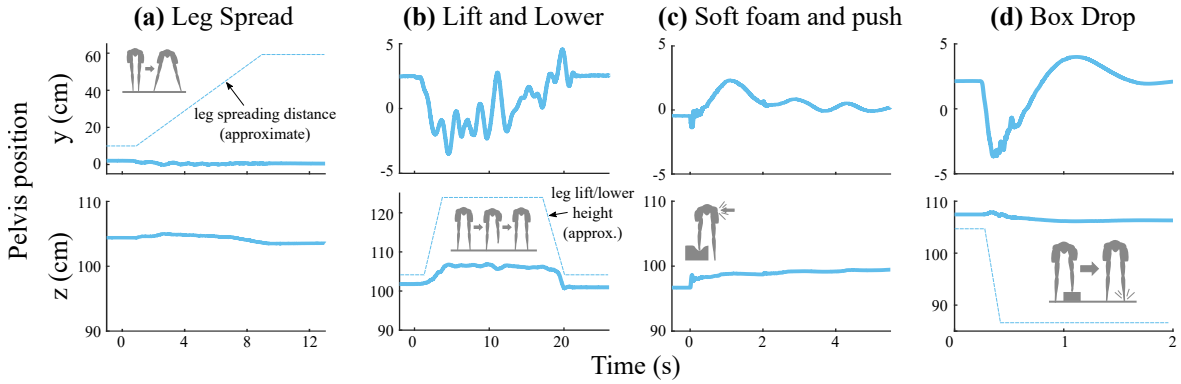

Fig. 7. Experimental data from each of four perturbation tests. (a) Cassie's foot is pulled away while maintaining a stable height. (b) Cassie's foot is moved up and down and Cassie returns to its initial position. (c) Cassie is pushed on soft foam and returns to a stable position. (d) Cassie's foot falls rapidly as a box is pulled out from beneath its foot, and Cassie recovers to initial position. Solid lines are measured pelvis data, and dashed lines represent approximated leg perturbations (e.g. height of leg lift). Note: y-positions are measured as the distance from the desired centered position. See supplementary video for experimental footage.

V. Conclusions

The presented force-controlled balancing algorithm allowed Tallahassee Cassie to balance on uneven, moving, and soft surfaces - which we call dynamic terrain. Even when a contact point was swiftly removed by a pulling out a supporting box, the force controller quickly stomped the leg to a new contact point and recovered. The controller is realizable in part because of its hardware platform. Tallahassee Cassie is equipped with low-friction cycloidal drives transmissions (or transparency), and thus sufficiently high-fidelity torque control is possible. Further, Cassie's series springs protect the structure from impacts, allowing the controller to quickly and safely move to new contact points when the ground is pulled away.

We further note that this controller functioned in spite of the vastly simplifying assumptions made to implement the controller. Cassie has soft and passive series-elasticity in four joints, and significant mass and inertia in its long legs (especially compared to its compact torso). Yet, the total robot mass is assumed to be completely contained in the pelvis with the legs being massless, and the spring deflections are excluded from the kinematics computations. Additionally, there is no explicit modeling or control logic for swing phases, so any airborne behavior for a leg strictly emerges from the force controller. These control results are a foundation for further control on real-world terrain, including walking and running on dynamic terrain. Immediate next steps will seek to incorporate stepping logic to broaden the disturbance capability of the robot.

Acknowledgment

This work was supported by the Mechanical Engineering Department in the FAMU-FSU College of Engineering, the Florida State University Council on Research and Creativity, and the collaborative participation in the Robotics Consortium sponsored by the U.S. Army Research Laboratory under the Collaborative Technology Alliance Program, Cooperative Agreement DAAD 19-01-20012.

References

[1] M. Vukobratovic and D. Juricic, "Contribution to the synthesis of biped gait," *IEEE Transactions on Biomedical Engineering*, no. 1, pp. 1–6, 1969.

[2] S. Kajita, F. Kanehiro, K. Kaneko, K. Fujiwara, K. Harada, K. Yokoi, and H. Hirukawa, "Biped walking pattern generation by using preview control of zero-moment point," in *2003 IEEE International Conference on Robotics and Automation (Cat. No. 03CH37422)*, vol. 2. IEEE, 2003, pp. 1620–1626.

[3] G. Wiedebach, S. Bertrand, T. Wu, L. Fiorio, S. McCrory, R. Griffin, F. Nori, and J. Pratt, "Walking on partial footholds including line contacts with the humanoid robot atlas," in *2016 IEEE-RAS 16th International Conference on Humanoid Robots (Humanoids)*. IEEE, 2016, pp. 1312–1319.

[4] S. Kuindersma, R. Deits, M. Fallon, A. Valenzuela, H. Dai, F. Permenter, T. Koolen, P. Marion, and R. Tedrake, "Optimization-based locomotion planning, estimation, and control design for the ATLAS humanoid robot," *Autonomous Robots*, vol. 40, no. 3, pp. 429–455, 2016.

[5] S. Feng, X. Xinjilefu, C. G. Atkeson, and J. Kim, "Optimization based controller design and implementation for the ATLAS robot in the darpa robotics challenge finals," in *2015 IEEE-RAS 15th International Conference on Humanoid Robots (Humanoids)*. IEEE, 2015, pp. 1028–1035.

[6] M. Shrivastava, A. Dutta, and A. Saxena, "Trajectory generation using GA for an 8 dof biped robot with deformation at the sole of the foot," *Journal of Intelligent and Robotic Systems*, vol. 49, no. 1, pp. 67–84, 2007.

[7] A. Hereid, C. M. Hubicki, E. A. Cousineau, and A. D. Ames, "Dynamic humanoid locomotion: A scalable formulation for HZD gait optimization," *IEEE Transactions on Robotics*, vol. 34, no. 2, pp. 370–387, 2018.

[8] X. Xiong, A. D. Ames, and D. I. Goldman, "A stability region criterion for flat-footed bipedal walking on deformable granular terrain," in *2017 IEEE/RSJ International Conference on Intelligent Robots and Systems (IROS)*. IEEE, 2017, pp. 4552–4559.

[9] W. Bosworth, J. Whitney, S. Kim, and N. Hogan, "Robot locomotion on hard and soft ground: Measuring stability and ground properties in-situ," in *2016 IEEE International Conference on Robotics and Automation (ICRA)*. IEEE, 2016, pp. 3582–3589.

[10] N. Rotella, S. Schaal, and L. Righetti, "Unsupervised contact learning for humanoid estimation and control," in *2018 IEEE International Conference on Robotics and Automation (ICRA)*. IEEE, 2018, pp. 411–417.

[11] A. H. Chang, C. Hubicki, A. Ames, and P. A. Vela, "Every hop is an opportunity: Quickly classifying and adapting to terrain during targeted hopping," in *2019 International Conference on Robotics and Automation (ICRA)*. IEEE, 2019, pp. 3188–3194.

[12] H.-j. Kang, K. Hashimoto, K. Nishikawa, E. Falotico, H.-o. Lim, A. Takanishi, C. Laschi, P. Dario, and A. Berthoz, "Biped walking stabilization on soft ground based on gait analysis," in *2012 4th IEEE RAS & EMBS International Conference on Biomedical Robotics and Biomechatronics (BioRob)*. IEEE, 2012, pp. 669–674.

[13] N. Paine, J. S. Mehling, J. Holley, N. A. Radford, G. Johnson, C.-L. Fok, and L. Sentis, "Actuator control for the NASA-JSC valkyrie humanoid robot: A decoupled dynamics approach for torque control of series elastic robots," *Journal of Field Robotics*, vol. 32, no. 3, pp. 378–396, 2015.

[14] J. Englsberger, A. Werner, C. Ott, B. Henze, M. A. Roa, G. Garofalo, R. Burger, A. Beyer, O. Eiberger, K. Schmid, *et al.*, "Overview of the torque-controlled humanoid robot toro," in *2014 IEEE-RAS International Conference on Humanoid Robots*. IEEE, 2014, pp. 916–923.

[15] B. Henze, M. A. Roa, and C. Ott, "Passivity-based whole-body balancing for torque-controlled humanoid robots in multi-contact scenarios," *The International Journal of Robotics Research*, vol. 35, no. 12, pp. 1522–1543, 2016.

[16] D. Kim, Y. Zhao, G. Thomas, B. R. Fernandez, and L. Sentis, "Stabilizing series-elastic point-foot bipeds using whole-body operational space control," *IEEE Transactions on Robotics*, vol. 32, no. 6, pp. 1362–1379, 2016.

[17] D. Kim, S. J. Jorgensen, H. Hwang, and L. Sentis, "Control scheme and uncertainty considerations for dynamic balancing of passive-ankled bipeds and full humanoids," in *2018 IEEE-RAS 18th International Conference on Humanoid Robots (Humanoids)*. IEEE, 2018, pp. 1–9.

[18] O. Khatib, "A unified approach for motion and force control of robot manipulators: The operational space formulation," *IEEE Journal on Robotics and Automation*, vol. 3, no. 1, pp. 43–53, 1987.

[19] J. Di Carlo, P. M. Wensing, B. Katz, G. Bledt, and S. Kim, "Dynamic locomotion in the MIT cheetah 3 through convex model-predictive control," in *2018 IEEE/RSJ International Conference on Intelligent Robots and Systems (IROS)*. IEEE, 2018, pp. 1–9.

[20] F. Jenelten, J. Hwangbo, F. Tresoldi, C. D. Bellicoso, and M. Hutter, "Dynamic locomotion on slippery ground," *IEEE Robotics and Automation Letters*, vol. 4, no. 4, pp. 4170–4176, 2019.

[21] C. Hubicki, A. Abate, P. Clary, S. Rezazadeh, M. Jones, A. Peekema, J. Van Why, R. Domres, A. Wu, W. Martin, *et al.*, "Walking and running with passive compliance: Lessons from engineering: A live demonstration of the ATRIAS biped," *IEEE Robotics & Automation Magazine*, vol. 25, no. 3, pp. 23–39, 2018.

[22] X. Da and J. Grizzle, "Combining trajectory optimization, supervised machine learning, and model structure for mitigating the curse of dimensionality in the control of bipedal robots," *The International Journal of Robotics Research*, vol. 38, no. 9, pp. 1063–1097, 2019.

[23] Z. Xie, P. Clary, J. Dao, P. Morais, J. Hurst, and M. van de Panne, "Iterative reinforcement learning based design of dynamic locomotion skills for cassie," *arXiv preprint arXiv:1903.09537*, 2019.

[24] X. Xiong and A. D. Ames, "Coupling reduced order models via feedback control for 3d underactuated bipedal robotic walking," in *2018 IEEE-RAS 18th International Conference on Humanoid Robots (Humanoids)*. IEEE, 2018, pp. 1–9.

[25] Y. Gong, R. Hartley, X. Da, A. Hereid, O. Harib, J.-K. Huang, and J. Grizzle, "Feedback control of a cassie bipedal robot: Walking, standing, and riding a segway," in *Proceedings of the American Control Conference*, 2019.